Heart and Vessels (2019) 34:724–734
https://doi.org/10.1007/s00380-018-1304-4

ORIGINAL ARTICLE

Type 2 inositol 1,4,5-trisphosphate receptor inhibits the progression of pulmonary arterial hypertension via calcium signaling and apoptosis

Akimichi Shibata[1,2] · Keiko Uchida[1,2,3] · Kazuki Kodo[1,2] · Takayuki Miyauchi[4] · Katsuhiko Mikoshiba[5] · Takao Takahashi[1] · Hiroyuki Yamagishi[1,2]

Received: 11 September 2018 / Accepted: 9 November 2018 / Published online: 20 November 2018

Abstract

Pulmonary arterial hypertension (PAH) is a progressive disease associated with vasoconstriction and remodeling. Intracellular Ca^{2+} signaling regulates the contraction of pulmonary arteries and the proliferation of pulmonary arterial smooth muscle cells (PASMCs); however, it is not clear which molecules related to Ca^{2+} signaling contribute to the progression of PAH. In this study, we found the specific expression of type 2 inositol 1,4,5-trisphosphate receptor (IP_3R2), which is an intracellular Ca^{2+} release channel, on the sarco/endoplasmic reticulum in mouse PASMCs, and demonstrated its inhibitory role in the progression of PAH using a chronic hypoxia-induced PAH mouse model. After chronic hypoxia exposure, $IP_3R2^{-/-}$ mice exhibited the significant aggravation of PAH, as determined by echocardiography and right ventricular hypertrophy, with significantly greater medial wall thickness by immunohistochemistry than that of wild-type mice. In $IP_3R2^{-/-}$ murine PASMCs with chronic hypoxia, a TUNEL assay revealed the significant suppression of apoptosis, whereas there was no significant change in proliferation. Thapsigargin-induced store-operated Ca^{2+} entry (SOCE) was significantly enhanced in $IP_3R2^{-/-}$ PASMCs in both normoxia and hypoxia based on in vitro fluorescent Ca^{2+} imaging. Furthermore, the enhancement of SOCE in $IP_3R2^{-/-}$ PASMCs was remarkably suppressed by the addition of DPB162-AE, an inhibitor of the stromal-interacting molecule (STIM)–Orai complex which is about 100 times more potent than 2-APB. Our results indicate that IP_3R2 may inhibit the progression of PAH by promoting apoptosis and inhibiting SOCE via the STIM–Orai pathway in PASMCs. These findings suggest a previously undetermined role of IP_3R in the development of PAH and may contribute to the development of targeted therapies.

Keywords Pulmonary artery smooth muscle cells · Chronic hypoxia · Store-operated calcium entry · Apoptosis

Introduction

Pulmonary arterial hypertension (PAH) is a progressive disease despite benefits from recently developed targeted therapies. PAH is characterized by increased pulmonary vascular resistance resulting primarily from vasoconstriction and the vascular remodeling of pulmonary arteries [1].

Ca^{2+} signaling and the Ca^{2+} concentration in pulmonary artery smooth muscle cells (PASMCs) play a major role in the regulation of vasoconstriction or the vascular remodeling of pulmonary arteries and are often associated with the progression of PAH. Membrane depolarization of PASMCs promotes Ca^{2+} influx via the voltage-dependent Ca^{2+} channel [2, 3]. Various stimuli of membrane receptors lead to the acceleration of Ca^{2+} entry into PASMCs through extracellular ligand binding on G protein-coupled

✉ Keiko Uchida
keiuchida@keio.jp

✉ Hiroyuki Yamagishi
hyamag@keio.jp

1 Department of Pediatrics, Keio University School of Medicine, 35 Shinanomachi, Shinjuku-ku, Tokyo 160-8582, Japan

2 Division of Cardiology, Keio University School of Medicine, Tokyo, Japan

3 Health Center, Keio University, Kanagawa, Japan

4 Department of Pharmacology, Keio University School of Medicine and Keio Advanced Research Center for Water Biology and Medicine, Keio University, Tokyo, Japan

5 The Laboratory for Developmental Neurobiology, RIKEN Center for Brain Science, Saitama, Japan

receptors (GPCRs) or receptor tyrosine kinases (RTKs) [2]. Ca^{2+} entry occurs by two major mechanisms related to these receptors on the membranes of PASMCs, i.e., receptor-operated Ca^{2+} entry (ROCE) and store-operated Ca^{2+} entry (SOCE). ROCE is regulated by diacylglycerol (DAG) [4–6]. When phospholipase C is activated by GPCRs or RTKs, the production of DAG and inositol 1,4,5-trisphosphate (IP_3) is activated. DAG can open receptor-operated Ca^{2+} channels (ROC), leading to Ca^{2+} entry into PASMCs. Alternatively, Ca^{2+} depletion in the sarco/endoplasmic reticulum (SR/ER) induced by Ca^{2+} release also leads to Ca^{2+} influx in a process referred to as SOCE [4, 7]. When stromal-interacting molecule (STIM) on the SR/ER membrane senses Ca^{2+} depletion, it translocates to the SR/ER-plasma membrane junction and induces Ca^{2+} influx via Orai [8].

IP_3 receptor (IP_3R), which is an intracellular Ca^{2+} release channel resident on the SR/ER, also contributes to SOCE in PASMCs by leading to Ca^{2+} store depletion [2]. IP_3R communicates with many ion channels or intracellular organelles that regulate the elevation of intracellular Ca^{2+} concentration or vasoconstriction [9, 10]. There are three subtypes of IP_3R (IP_3R1, 2, and 3) with versatile roles in pathophysiology in many organs [9, 10]. IP_3R2 is expressed at relatively high levels in the lungs, testis, heart, and liver [11]. IP_3R2 mutations in humans disrupt sweat secretion [12]. IP_3R2 and IP_3R3 are required for exocrine fluid secretion, including saliva, pancreatic juice, and tears [13, 14]. In the cardiovascular system, the overexpression of IP_3R2 in the heart results in hypertrophy of the cardiac muscle [15]. All subtypes of IP_3R are expressed in the cardiovascular system from the embryonic to postnatal periods, suggesting their genetic redundancy, and we previously reported that IP_3R1–IP_3R2 or IP_3R1–IP_3R3 double-knockout mice die around embryonic day 11.5 due to various disorders during cardiovascular development [16–18]. However, the role of IP_3R in the lungs or lung vasculature is poorly understood, although it may affect vasoconstriction or remodeling in vascular smooth muscle cells [19].

In this study, we investigated the role of IP_3R2 in the development of PAH using hypoxia-induced PAH mouse models both in vivo and in vitro. Our data suggest an inhibitory role of IP_3R2 in the progression of PAH by its pro-apoptotic function and the suppression of SOCE via STIM–Orai interactions.

Materials and methods

Animals and tissues

Experiments were performed in mice or embryos homozygous null for IP_3R2 ($IP_3R2^{-/-}$; KO), generated by intercrossing $IP_3R2^{+/-}$ mice [14] after repeating the cross to C57BL/6J mice more than ten times. In addition, C57BL/6J wild-type mice or embryos were used for control. All experimental procedures and protocols were performed in accordance with animal protocols approved by the Institutional Animal Care and Use Committees of Keio University [approval number 9122-(10)] and conformed to the National Institutes of Health Guidelines for the Care and Use of Laboratory Animals.

Hypoxia-induced PAH mice models

Adult male $IP_3R2^{-/-}$ mice or wild-type (C57BL/6J) mice were housed under controlled conditions with free access to rodent chow and tap water. To gain chronic hypoxia-induced-PAH mice, those were kept for 8 weeks under normobaric hypoxia (10% O_2) [20] until transthoracic echocardiography or tissue sampling. Control mice were kept under normobaric normoxia (room air) conditions and were fed standard diet for the entire study period.

Echocardiography

Mice were continuously anesthetized by 1.5–2% of isoflurane inhalant mixed with 1 l/min 100% O_2 to maintain a light sedation level throughout the procedure of transthoracic echocardiography. They were immobilized on a heating platform ventral side up to maintain the body temperature at 37 °C ± 0.5 °C. Heart rate and respiratory physiology were continuously monitored by ECG electrodes. The chests of the mice were shaved, and warmed ultrasound gel was applied to the area of interest. Transthoracic echocardiography was performed using a Vevo 2100 system (VisualSonics, Toronto, Canada) with a 38-MHz transducer. Care was taken to avoid excessive pressure over the sternum, which can distort the signal. Images were captured on cine loops at the time of the study and afterward measurements were done offline. The ratio of acceleration time to ejection time (AcT/ET) of pulmonary arteries and the left ventricular eccentricity index (LVEI) provided by echocardiography was also evaluated for the severity of PAH [21, 22]. After echocardiography, the dissected right ventricles were weighed and fixed for preparation of paraffin sections.

Whole-mount and section LacZ staining

We performed whole-mount LacZ (β-galactosidase) staining of the lungs isolated from $IP_3R2^{-/-}$ mice, harboring *LacZ* gene in-frame at the translation initiation site of the IP_3R2 locus, after fixation with 2%-PFA 0.1%-glutaraldehyde followed by clearing with benzyl alcohol–benzyl benzoate, as described previously with minor modifications [23]. To improve permeability of the substrate, X-gal, we used rinse buffer (0.2M sodium phosphate, pH 7.3, 2 mM $MgCl_2$,

0.01% sodium deoxycholate, 0.02% NP-40) for washing. After whole-mount LacZ staining, the tissue specimens were postfixed, dehydrated, and embedded in paraffin.

Immunohistochemistry staining

The mice lung paraffin sections were made at 7-μm intervals, mounted onto slide glasses, and used for immunohistochemistry. Section immunohistochemistry was performed with anti-α-smooth muscle actin (αSMA) (1:400, 1A4; Sigma) and anti-von Willebrand Factor (vWF) (1:200, Ab-1; Thermo scientific) as described previously [16]. Fluorescent images were observed under the fluorescence microscope, BX50 (Olympus), and captured with the colored CCD camera, DFC300FX (Leica).

TUNEL and cell-proliferation assays

TUNEL staining and proliferation assays were performed on transverse paraffin sections from 8-week conditioned adult mice lungs according to the previous report [17]. The ApopTag Fluorescein in situ apoptosis detection kit (Merck) was used for TUNEL assays. Proliferation assays were performed by immunohistochemistry with anti-phosphohistone H3 (Ser10), a mitosis marker, antibody (1:200, Millipore) as a primary antibody [17].

Primary culture of mouse pulmonary artery smooth muscle cells (PASMCs)

Pulmonary artery smooth muscle cells (PASMCs) were isolated from the wild-type and $IP_3R2^{-/-}$ mice as previously reported with some modifications [24]. Mice pulmonary arteries from first to third branches, containing intra-lobular arteries, were isolated carefully from embryos at E18.5 under stereoscopic microscope. The dissected tissues were dissociated and cultured as previously reported [24]. Cell suspensions were transferred to growth medium, containing DMEM with 10% FBS, 100 U/ml penicillin, and 100 mg/ml streptomycin (Invitrogen), in 35-mm poly-L-lysine (Sigma) coated, glass-bottomed dishes (MatTek) in a moist tissue culture incubator at 37 °C in 5% CO_2-95% ambient mixed air. The subconfluent cells were used for Ca^{2+} imaging. We confirmed that cells were positive for αSMA by immunostaining and showed the typical "hill-and-valley" morphology.

Ca^{2+} imaging

After 4-day primary culture of the PASMCs, dishes were randomly divided into normoxic or hypoxic condition. Hypoxic dishes were incubated in 4% O_2/5% CO_2 (Anaeropack, Sugiyama-gen) at 37 °C, whereas normoxic dishes kept in 5% CO_2-95% ambient mixed air, then incubated for additional 1-day culture. A Ca^{2+}-sensitive fluorescence indicator, Fluo-4 AM (Dojindo), was mixed with Pluronic F-127 and Cremophor EL by sonication. PASMCs were loaded with 10-μM Fluo-4 AM at 37 °C for 30 min in balanced salt solution containing 115-mM NaCl, 5.4-mM KCl, 2-mM $CaCl_2$, 1-mM $MgCl_2$, 20-mM HEPES, and 10-mM glucose, pH 7.4 (BSS^+) [25]. To assess SOCE, extracellular Ca^{2+} was removed with Ca^{2+}-free recording medium (BSS^+ without $CaCl_2$, BSS^-) which contains 10-μM nifedipine for the inhibition of L-type Ca^{2+} channels. Ca^{2+} measurement was carried out in BSS^- at room temperature. Imaging of Fluo-4 fluorescence in cells was performed using a FV1000 confocal microscope equipped with a 60 ×/1.2 NA water-immersion objective (Olympus) [26]. Excitation at 488 nm was assessed by a photomultiplier through 500- to 600-nm grating-based spectroscopy. Images in an experiment were acquired every 5 s per 1 frame for 30 min and analyzed using the custom Fluoview software (Olympus). In all experiments, multiple cells were imaged in a single field. Intracellular Ca^{2+} concentration changes were presented as F/F_0, where F is the mean values of fluorescence intensity in one arbitrarily chosen peripheral cytosolic area from each cell and F_0 is the baseline as calculated by averaging 12 frames for 60 s at minimum resting level. SOCE and ROCE were elicited immediately after the addition of extracellular Ca^{2+} (2 mM $CaCl_2$) to medium, following the precede addition of 10-μM thapsigargin for Ca^{2+} depletion of Ca^{2+} store and 100-μM oleoyl-acyl-sn-glycerol (OAG) for activation of receptor, respectively. Relative mobilizations of Ca^{2+} levels were estimated from the area under the curve (AUC) of the F/F_0 traces for 5 min after the addition of extracellular Ca^{2+} as the standardized value of the Ca^{2+} entry [27]. Each experiment was followed by the addition of 3.7 μM ionomycin and 5 mM EGTA to confirm maximum and minimum fluorescent intensities, respectively. DPB162-AE was used as a selective inhibitor for STIM–Orai interaction [28, 29].

Statistics

Results are expressed as the mean ± SE. p values < 0.05 were considered statistically significant for two-way ANOVA analysis, followed by Tukey's post hoc test, as appropriate (SPSS ver. 25).

Results

IP_3R2 is highly expressed in smooth muscle cells of pulmonary arteries

In an analysis of $IP_3R2^{-/-}$ mice harboring the *LacZ* gene in-frame at the translation initiation site of the IP_3R2

locus, we found that IP_3R2 was continuously expressed from the central to peripheral pulmonary artery (PA) based on whole-mount LacZ staining on the lungs (Fig. 1A). To clarify which cell type expressed IP_3R2 in the PA, adult cryosections of $IP_3R2^{-/-}$ mouse lungs were stained with LacZ, anti-αSMA, and anti-vWF antibodies simultaneously. IP_3R2 was located exclusively in PASMCs but not in bronchial smooth muscles (Fig. 1B) that was reminiscent of its endogenous expression pattern (data not shown).

PAH induced by chronic hypoxia was significantly aggravated in $IP_3R2^{-/-}$ mice

To determine whether a loss of IP_3R2 plays a role in PAH, C57BL/6J wild-type and $IP_3R2^{-/-}$ mice were kept in a 10% O_2 chamber for 8 weeks to obtain a chronic hypoxia-induced PAH mouse model [20]. Their cardiopulmonary function and specimens were analyzed and compared with those kept in room air (normoxia) (Fig. 2A). The mean AcT/ET and end-systolic LVEI were determined by echocardiography. AcT/ET was significantly lower in wild-type mice under hypoxia than under normoxia (Fig. 2B, $p = 0.001$), and LVEI was also

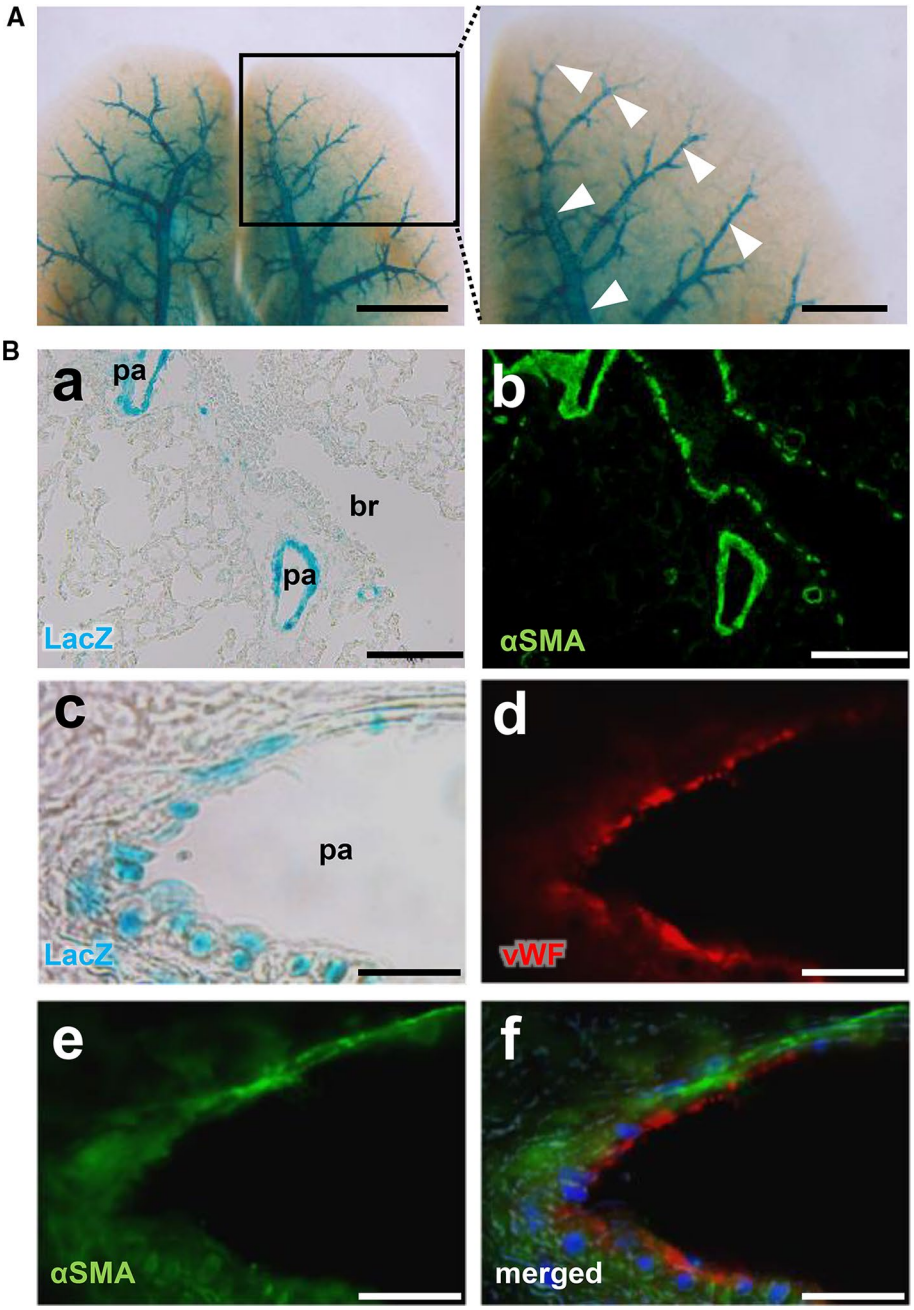

Fig. 1 Expression of IP_3R2 in mouse PASMCs. **A** Whole-mount LacZ staining of lungs obtained from $IP_3R2^{-/-}$ mice just before birth (embryonic day 19.5) is shown. Right panel shows a higher magnification view of the inset in the left panel. The expression of IP_3R2 in the pulmonary arteries (pa) is shown in blue (arrowheads). Scale bars 1 mm (left panel), 0.5 mm (right panel). **B** Simultaneous staining of LacZ (a) and anti-α-smooth muscle actin (αSMA) (b) of the postnatal 16-day $IP_3R2^{-/-}$ mouse lung cryosection shows that IP_3R2 is expressed only in the pa in blue (a), whereas immunohistochemistry with an anti-αSMA antibody detects smooth muscle cells in both pa and bronchi (br) in green color (b). The simultaneous staining of LacZ (c) and immunohistochemistry with anti-von Willebrand factor (vWF) (d) and anti-αSMA antibodies (e) of adult $IP_3R2^{-/-}$ mouse lung sections and the merged image (f) shows the specific expression of IP_3R2 in smooth muscle cells in the tunica media of pa in blue (c and f), the vWF positive endothelial cells in red (d and f), and the αSMA-positive smooth muscle cells in green (e and f). Scale bars 100 μm in a and b; 20 μm in c, d, e, and f

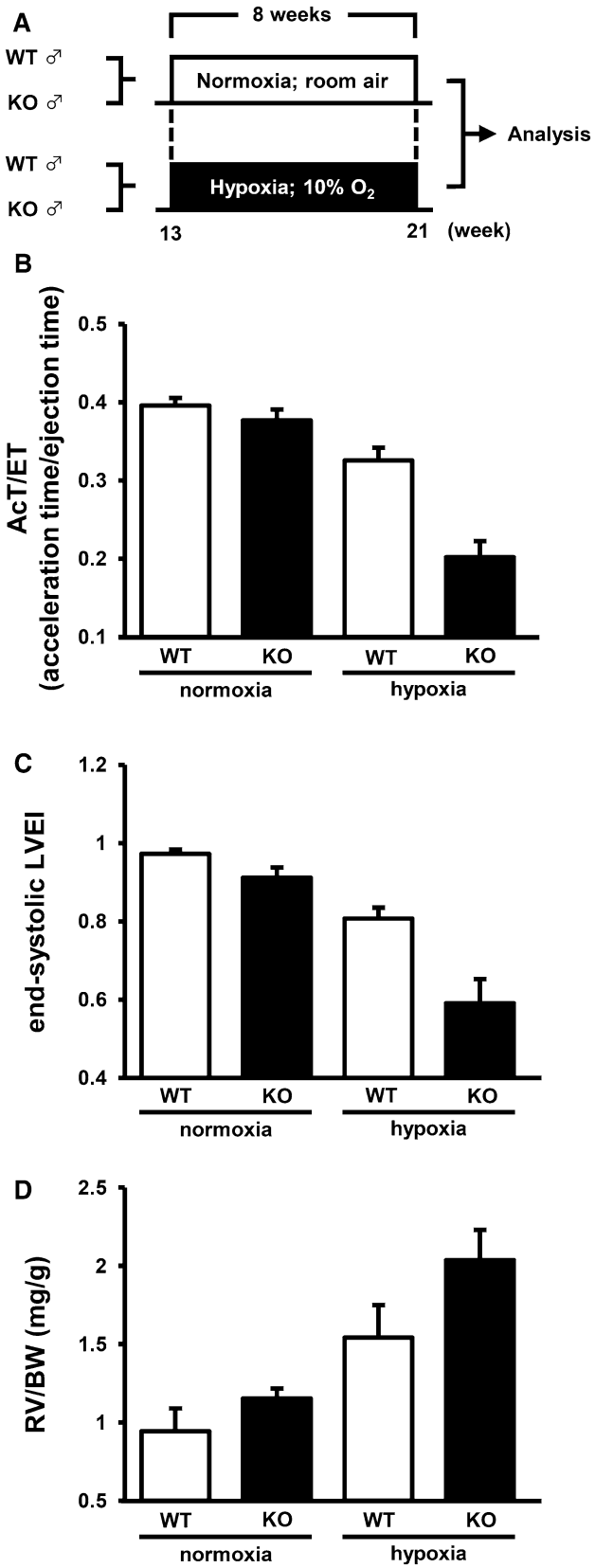

Fig. 2 Chronic hypoxia-induced PAH was significantly aggravated in ▶ $IP_3R2^{-/-}$ mice. **A** Experimental protocol for the in vivo evaluation of PAH for mice with chronic hypoxia. **B** Measurement of the pulmonary outflow velocity by pulse wave color Doppler imaging to calculate the ratio of the acceleration time to ejection time (AcT/ET). A lower value indicates more severe PAH. **C** Measurement of left ventricular eccentricity index (LVEI) at end-systole. A lower value indicates more severe PAH. **D** Analysis of right ventricular (RV) hypertrophy by the ratio of RV weight to whole body weight (RV/BW) ($n=4$ mice in each group). A higher value indicates more severe PAH. Data are shown as means ± SEM. **B** Two-way ANOVA, followed by Tukey's test. $p=0.025$ (wild type + normoxia vs. wild type + hypoxia), $p=0.000$ ($IP_3R2^{-/-}$+ normoxia vs. $IP_3R2^{-/-}$+ hypoxia and wild type + hypoxia vs. $IP_3R2^{-/-}$+ hypoxia). **C**, **D** Two-way ANOVA. p = 0.000 (normoxia vs. hypoxia), $p=0.003$ (wild type vs. $IP_3R2^{-/-}$) (**c**), and $p=0.000$ (normoxia vs. hypoxia), $p=0.001$ (wild type vs. $IP_3R2^{-/-}$) (**D**). WT, wild-type mice; KO, $IP_3R2^{-/-}$ mice. To avoid the bias of respiratory variation, all data were gained by measuring more than two times from 4 mice ($n=8$–14 heart beats) in each group (**B**, **C**)

significantly lower under hypoxia than normoxia (Fig. 2C, $p=0.000$), suggesting that PAH was induced by this protocol. Although AcT/ET was comparable in wild-type and $IP_3R2^{-/-}$ mice with normoxia, they were significantly lower in the $IP_3R2^{-/-}$ mice than in wild-type mice with hypoxia (Fig. 2B, $p=0.000$). After echocardiography, murine lungs and hearts were dissected and right ventricle (RV) hypertrophy was assessed, where the RV weight of each mouse was adjusted by the individual body weight (RV/BW) [30]. RV/BW was significantly greater in the hypoxia group than in the normoxia group in both wild-type and $IP_3R2^{-/-}$ mice and was significantly greater in $IP_3R2^{-/-}$ mice than in wild-type mice with hypoxia (Fig. 2D, $p=0.000$ for normoxia vs. hypoxia in both wild-type mice and $IP_3R2^{-/-}$ mice; $p=0.001$ for wild type vs. $IP_3R2^{-/-}$ in both normoxia and hypoxia). These data suggest that 8 weeks of hypoxia exposure successfully induced PAH in mice and that PAH was significantly aggravated by a loss of IP_3R2.

Medial wall of the PA was significantly thickened in $IP_3R2^{-/-}$ mice with chronic hypoxia

As IP_3R2 was exclusively expressed in PASMCs of the medial wall of the PA, we evaluated medial wall thickness in wild-type and $IP_3R2^{-/-}$ mice with normoxia or hypoxia (Fig. 3A). The medial wall area adjusted for the vascular internal diameter was calculated. Medial wall thickness was significantly greater in $IP_3R2^{-/-}$ mice with hypoxia than in wild-type mice ($p=0.000$ for normoxia vs. hypoxia, $p=0.000$ for wild type vs. $IP_3R2^{-/-}$) (Fig. 3B).

Next, we examined whether alterations in apoptosis or proliferation in PASMCs contribute to the medial wall thickness in $IP_3R2^{-/-}$ mice. Apoptosis was evaluated by a TUNEL assay of lung paraffin sections obtained from the same groups of mice in normoxic or hypoxic conditions

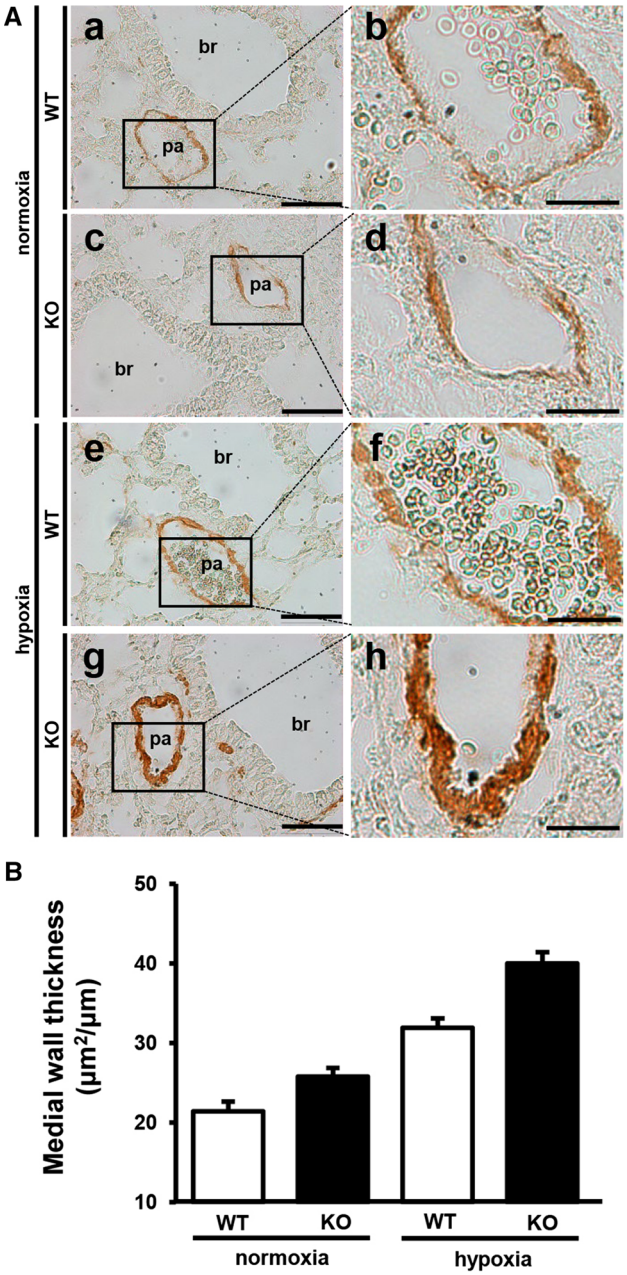

Fig. 3 Medial wall thickness of PA was significantly increased in $IP_3R2^{-/-}$ mice. **A** Representative images of immunohistochemistry with an anti-αSMA antibody on lung paraffin sections of wild-type mice (WT) (a, b) and $IP_3R2^{-/-}$ mice (KO) (c, d) with normoxia and WT (e, f) and KO mice (g, h) with hypoxia. b, d, f, and h are higher magnification views of the insets in a, c, e, and g, respectively. Smooth muscle cells are stained in brown. br, bronchus; pa, pulmonary artery. Scale bars 50 μm (a, c, e, and g), 20 μm (b, d, f, and h). **B** Medial wall thicknesses of PA calculated by the mean ratio of the PASMC area to each vascular internal diameter are shown in a bar graph ($n = 93$–155 pulmonary artery sections from 4 mice in each group). Data are shown as means ± SEM. Two-way ANOVA. $p = 0.000$ (normoxia vs. hypoxia), $p = 0.000$ (wild type vs. $IP_3R2^{-/-}$)

used for in vivo analyzes, and PASMCs were detected by anti-αSMA antibody staining (Fig. 4A). The number of TUNEL-positive PASMCs per unit area (square-centimeter), determined by fluorescent microscopy, was lower in chronic hypoxia-induced PAH mice and was significantly lower in $IP_3R2^{-/-}$ mice than in wild-type mice with both normoxia and hypoxia (Fig. 4B, $p = 0.003$ for normoxia vs. hypoxia, $p = 0.000$ for wild type vs. $IP_3R2^{-/-}$).

The proliferation of PASMCs was assessed by anti-phosphohistone H3 (PHH3) antibody staining (Fig. 4C). The number of PHH3-positive cells in PASMCs was significantly higher in chronic hypoxia-induced PAH mice than in normoxia mice, whereas there was no significant difference between wild-type and $IP_3R2^{-/-}$ mice (Fig. 4D, $p = 0.000$ and 0.708, respectively). Taken together, these results suggest that apoptosis is significantly suppressed in PASMCs of $IP_3R2^{-/-}$ mice with chronic hypoxia, despite no remarkable change in proliferation, resulting in increased medial wall thickness in PA.

SOCE is enhanced in PASMCs with a loss of IP_3R2 and chronic hypoxia depending on the STIM–Orai pathway

Because IP_3R2 was expressed in mouse PASMCs and chronic hypoxia-induced PH was significantly aggravated in $IP_3R2^{-/-}$ mice, it is possible that alterations in Ca^{2+} mobilization in $IP_3R2^{-/-}$ PASMCs contributed to the progression of medial wall thickness in PAs and the aggravation of PH. For in vitro Ca^{2+} imaging, we isolated PASMCs from wild-type and $IP_3R2^{-/-}$ murine embryos at embryonic day 18.5 as previously described [24]. The primary cultured PASMCs were evaluated by Ca^{2+} imaging after 24-h culture under normoxia or hypoxia (Fig. 5). The intracellular Ca^{2+} concentration, estimated as the fluorescence intensity relative to baseline, or F/F_0, exhibited a slight transient elevation after the addition of thapsigargin, which is an inhibitor of Ca^{2+} uptake into intracellular Ca^{2+} stores via sarco/endoplasmic reticulum Ca^{2+}-ATPase, and a large increase in Ca^{2+} concentration was observed just after the addition of extracellular Ca^{2+} as reported previously [28]. The area under the curve of the F/F_0 traces for 5 min after the addition of extracellular Ca^{2+} in each experiment was calculated as the standardized Ca^{2+} entry value. Ca^{2+} entry was significantly greater in PASMCs with hypoxia and was more remarkable in $IP_3R2^{-/-}$ PASMCs than in wild-type PASMCs (Fig. 5A, B, $p = 0.000$ for normoxia vs. hypoxia, $p = 0.000$ for wild type vs. $IP_3R2^{-/-}$). In contrast, there was no significant difference in OAG-induced Ca^{2+} entry (ROCE) between wild-type and $IP_3R2^{-/-}$ PASMCs with either normoxia or hypoxia (Fig. 5C, D, $p = 0.050$ for wild type vs. $IP_3R2^{-/-}$). There also was no significant difference in SOCE between wild type and $IP_3R3^{-/-}$ PASMCs ($p = 0.183$ (data not shown)).

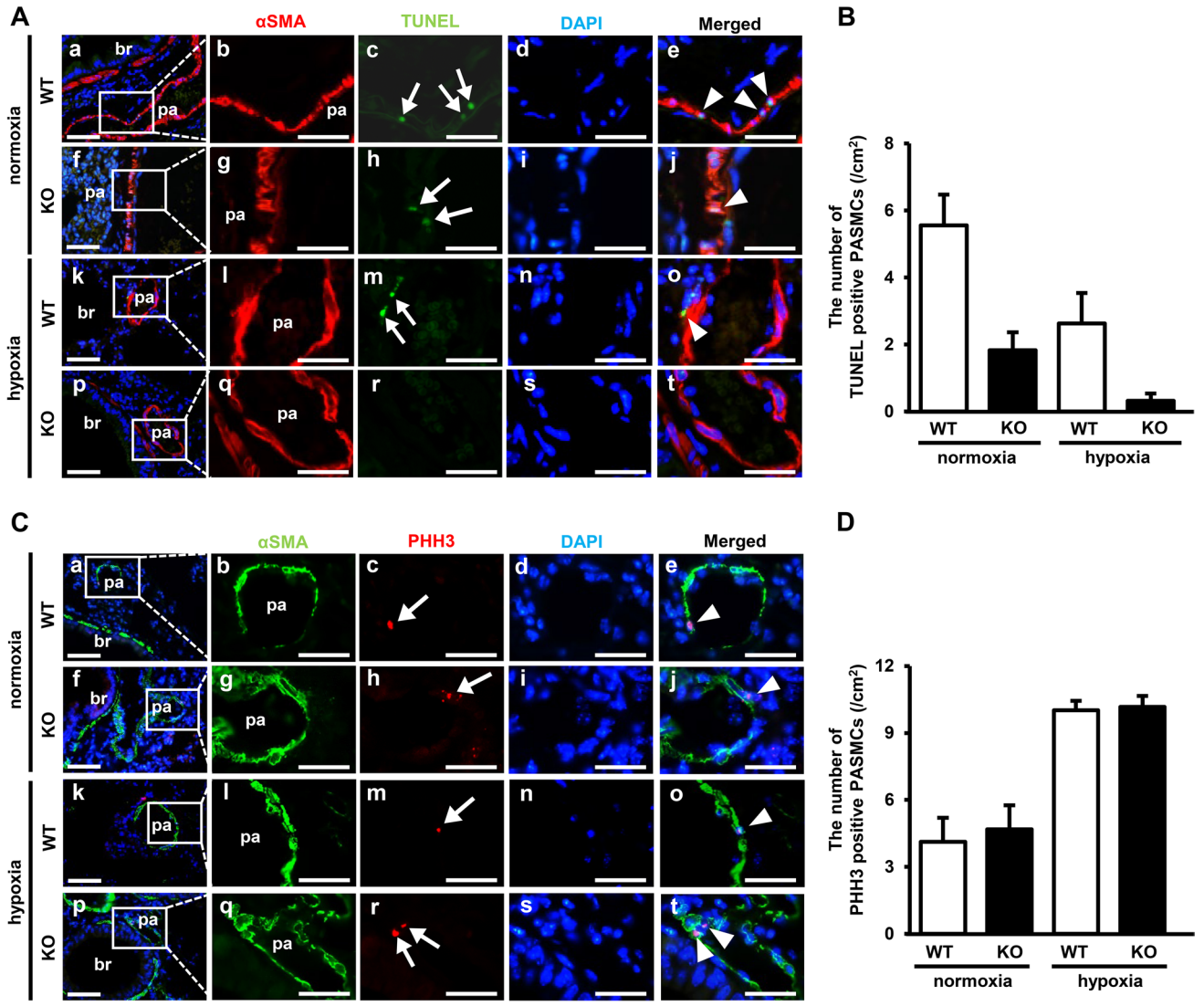

Fig. 4 Apoptosis, but not cell proliferation, was significantly altered in $IP_3R2^{-/-}$ PASMCs. **A** Mouse lung paraffin sections of each genotype and oxygen condition [a–e, wild type (WT) with normoxia; f–j, $IP_3R2^{-/-}$ (KO) with normoxia; k–o, WT with hypoxia; p–t, KO with hypoxia] with simultaneous staining of an anti-αSMA antibody (red in b, g, l, and q) and TUNEL (green in c, h, m, and r). Arrows indicate TUNEL-positive cells (c, h, and m) and arrowheads indicate TUNEL-positive PASMCs in merged images (e, j, and o). b–e, g–j, l–o, and q–t are higher magnification views of the insets in a, f, k, and p, respectively. **B** Bar graph shows the number of TUNEL-positive cells per unit area (cm^2) ($n = 9$–10 lung sections from 4 mice in each group). **C** Mouse lung paraffin sections in each genotype and oxygen condition (a–e, WT with normoxia; f–j, KO with normoxia; k–o, WT with hypoxia; p–t, KO with hypoxia) with simultaneous staining of the anti-αSMA antibody (green in b, g, l, and q) and anti-phosphohistone-H3 (PHH3) antibody (red in c, h, m, and r). Arrows indicate anti-PHH3-positive cells (c, h, m, and r) and arrowheads indicate anti-PHH3-positive PASMCs in merged images (e, j, o, and t). b–e, g–j, l–o, and q–t are higher magnification views of the insets in a, f, k, and p, respectively. **D** Bar graph shows the number of anti-PHH3 antibody-positive cells per unit area (cm^2) ($n = 4$–6 lung sections from 4 mice in each group). Scale bars 100 μm in a, f, k, and p of (**A**, **C**), 50 μm in b–e, g–j, l–o, q–t of (**A**, **C**). Data are shown as means ± SEM. Two-way ANOVA. $p = 0.003$ (normoxia vs. hypoxia), $p = 0.000$ (wild type vs. $IP_3R2^{-/-}$) (**B**), and $p = 0.000$ (normoxia vs. hypoxia), $p = 0.708$ (wild type vs. $IP_3R2^{-/-}$) (**D**)

To elucidate the molecular pathway involved in the enhancement of SOCE in $IP_3R2^{-/-}$ PASMCs, thapsigargin-induced SOCE was evaluated using the STIM–Orai inhibitor DPB162-AE [28]. SOCE is mostly mediated by the STIM–Orai interaction in human PASMCs and its upregulation could be responsible for the progression of PAH [31]; however, the contribution of IP_3R to this molecular pathway in PASMCs is unknown. In an analysis of concentrations from 0.3 to 30 μM DPB162-AE (data not shown), we confirmed that 3 μM DPB162-AE effectively inhibited SOCE in primary cultured mouse PASMCs while maintaining cell survival. DMSO (1:1000 in recording buffer) was used as a control and DPB162-AE was added after Ca^{2+} depletion by the administration of thapsigargin. Representative data

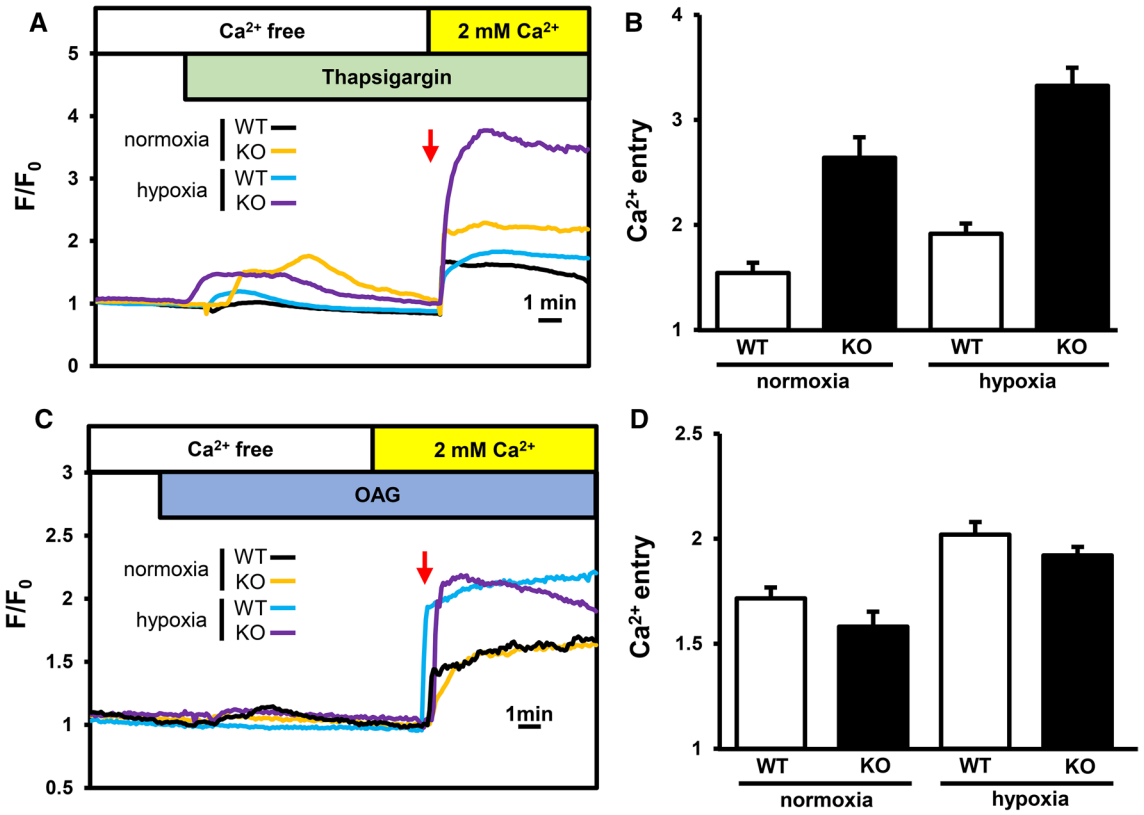

Fig. 5 SOCE was significantly increased in $IP_3R2^{-/-}$ PASMCs exposed to hypoxia. **A**, **B** SOCE in primary cultured PASMCs induced by thapsigargin. **C**, **D** ROCE in primary cultured PASMCs induced by OAG. Representative time course data of Ca^{2+} imaging for SOCE (**A**) and ROCE (**C**) of wild-type (WT) or $IP_3R2^{-/-}$ (KO) PASMCs with normoxia or hypoxia are shown. Ca^{2+} entry into PASMCs was elicited immediately after the addition of extracellular Ca^{2+} (arrows). The intracellular Ca^{2+} concentration is demonstrated by the fluorescence intensity relative to baseline, or F/F_0. F_0 and F represents the fluorescence intensities before and after the addition of thapsigargin (**A**) or OAG (**C**). Ca^{2+} entry was estimated from the area under the curve (AUC) of the F/F_0 traces for 5 min after the addition of extracellular Ca^{2+}. The bar graphs of the relative mobilization, referred to as Ca^{2+} entry, of SOCE (**B**) and ROCE (**D**) are shown. $n = 34–55$ cells from 3–4 independent experiments (**B**, **D**). Data are shown as means ± SEM. Two-way ANOVA. $p = 0.000$ (normoxia vs. hypoxia), $p = 0.000$ (wild type vs. $IP_3R2^{-/-}$) (**B**), and $p = 0.000$ (normoxia vs. hypoxia), $p = 0.050$ (wild type vs. $IP_3R2^{-/-}$) (**D**)

for Ca^{2+} entry with DPB162-AE or with DMSO revealed that SOCE in both wild-type and $IP_3R2^{-/-}$ PASMCs was significantly suppressed by DPB162-AE with either normoxia or hypoxia (Fig. 6A, B, $p = 0.000$ for wild type and $p = 0.000$ for $IP_3R2^{-/-}$ in normoxia; $p = 0.000$ for wild type and $p = 0.000$ for $IP_3R2^{-/-}$ in hypoxia). Taken together, these results indicate that the significant enhancement of SOCE in PASMCs as a result of a loss of IP_3R2 and chronic hypoxia is dependent on the STIM–Orai pathway.

Discussion

In this study, we demonstrated that IP_3R2 is critical for the regulation of Ca^{2+} homeostasis in PASMCs associated with PAH. IP_3R2 is a dominant subtype in the lungs [11]; we clarified that it is exclusively expressed in PASMCs but not in pulmonary arterial endothelial cells or bronchial smooth muscle cells. We have also found that the specific expression of IP_3R2 in PASMC is maintained during development (Ishizaki R, Uchida K, Yamagishi H. unpublished observation), and its expression in adult murine tissues were previously reported [11]. Given that IP_3R is an intracellular Ca^{2+} release channel and that increased intracellular Ca^{2+} leads to pulmonary vasoconstriction, which may contribute to the progression of PAH, we speculated that IP_3R2 expressed in PASMCs functions in the attenuation of PAH. To our surprise, a loss of function of IP_3R2 in mice exacerbated chronic hypoxia-induced PAH, resulting in hypertrophy of the tunica media in the PA. The knockdown of IP_3R1 in PASMCs attenuates intracellular Ca^{2+} influx in acute pulmonary hypoxic vasoconstriction [32]; however, IP_3R2 is thought to be involved in PAH by different mechanisms. Our analyzes revealed that the attenuation of apoptosis and the upregulation of thapsigargin-induced SOCE in $IP_3R2^{-/-}$ PASMCs are potential mechanisms.

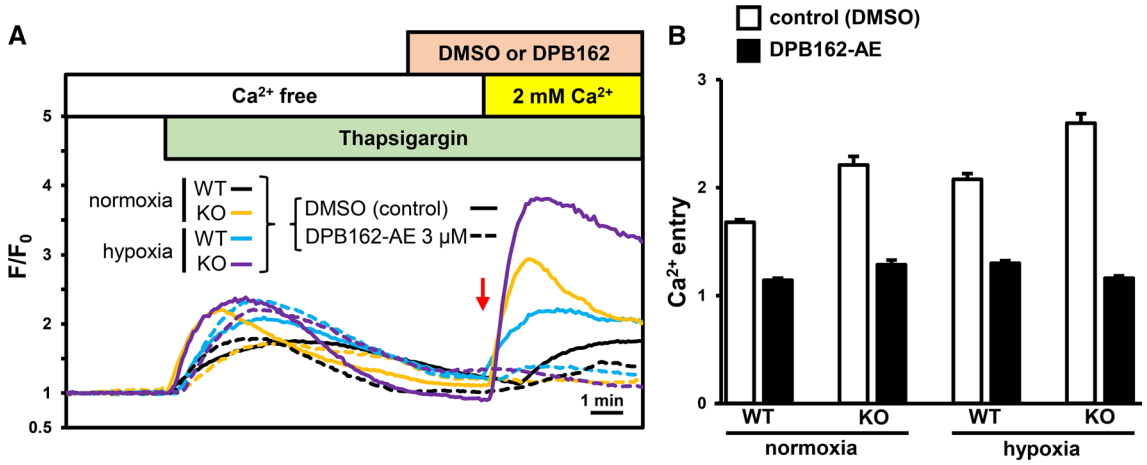

Fig. 6 Enhancement of SOCE in $IP_3R2^{-/-}$ PASMCs exposed to hypoxia was suppressed by a STIM–Orai inhibitor. **A** Representative time course data from Ca^{2+} imaging of SOCE in primary cultured PASMCs of wild type (WT) and $IP_3R2^{-/-}$ (KO) with normoxia or hypoxia with using DMSO as a control (solid lines) and the STIM–Orai inhibitor DPB162-AE (3 μM) (dashed lines). SOCE was elicited after the addition of extracellular Ca^{2+} (arrow). Similar to Fig. 5A, B, Ca^{2+} entry was estimated from the area under the curve (AUC) of the F/F_0 traces for 5 min after the addition of extracellular Ca^{2+}. **B** Bar graph of relative mobilization, referred to as Ca^{2+} entry, with control (white bars) and with DPB162-AE (black bars) is shown ($n = 32–52$ cells from 3–4 independent experiments). Data are shown as means ± SEM. Two-way ANOVA, followed by Tukey's post hoc test (**B**)

IP_3R2 in PASMCs promotes apoptosis

We detected the significant suppression of apoptosis in PASMCs in chronic hypoxia-induced PAH of $IP_3R2^{-/-}$ mice, whereas we did not observe a remarkable change in the proliferation of PASMCs. These results suggest a possible mechanism underlying the aggravation in chronic hypoxia-induced PAH of $IP_3R2^{-/-}$ mice, particularly in the context of numerous studies showing that the imbalance between apoptosis and proliferation of PASMCs is a major cause of PAH progression [1, 2]. This is consistent with a previously reported notion that three subtypes of IP_3R may be critical pro-apoptotic regulators of apoptosis mediated by (1) ER–mitochondrial junction complexes, (2) downstream Ca^{2+}-dependent signaling pathways related to apoptosis, and (3) a complex interaction between IP_3Rs and the Bcl-2 family [33]. Alternatively, apoptosis itself could be a stimulus to modulate IP_3R [34]. Furthermore, several studies have reported that IP_3R2 contributes to the apoptotic process in leukemic cells, interacting with anti-the apoptotic proteins Bcl-2 or Bcl-Xl [33, 35, 36]. Our results provide additional evidence that IP_3R2 has a pro-apoptotic function in mouse PASMCs with hypoxia-induced PAH.

IP_3R2 negatively regulates SOCE in PASMCs

Because intracellular Ca^{2+} signaling in PASMCs is a major regulator of pulmonary vasoconstriction and remodeling, leading to the progression of PAH [1, 2], we evaluated whether intracellular Ca^{2+} signaling is altered in our $IP_3R2^{-/-}$ mice with hypoxia-induced PAH. SOCE is upregulated in PASMCs in patients with PAH [37, 38], and the Ca^{2+} depletion of the SR/ER by Ca^{2+} release through IP_3R leads to the opening of SOC channels [39, 40]. Our results showed that thapsigargin-induced SOCE was significantly enhanced in $IP_3R2^{-/-}$ PASMCs compared to wild-type cells both in normoxia and hypoxia. We believe that the negative regulation of SOCE by IP_3R2 is specific, because there was no significant regulation of ROCE by IP_3R2 (Fig. 5C, D) or SOCE by IP_3R3 (data not shown). Therefore, the negative regulation of SOCE by IP_3R2 may be another possible mechanism underlying the aggravation of PAH in chronic hypoxia-induced PAH in $IP_3R2^{-/-}$ mice (Fig. 7).

Furthermore, we confirmed the role of STIM–Orai interaction in SOCE enhancement, indicated by a loss of IP_3R2, showing that SOCE was remarkably suppressed by the STIM–Orai inhibitor DPB162-AE and the enhancement of SOCE in $IP_3R2^{-/-}$ PASMCs was highly diminished. It was previously shown that the STIM–Orai interaction mediates Ca^{2+} signaling in PASMCs with hypoxia [41], and evidence for the negative regulation of SOCE by IP_3R has been reported in pancreatic acinar cells, where Orai and IP_3R are co-localized, although the function or contribution of individual subtypes of IP_3R remains unclear [42]. In PASMCs, IP_3R1 attenuates intracellular Ca^{2+} by a different mechanism [32] and IP_3R3 had no effect on SOCE in the present study (data not shown). In addition, we did not observe any upregulation of IP_3R1 or IP_3R3 expression in the IP_3R2-knockout lungs, indicating no genetic redundancy of either IP_3R1 or IP_3R3 for IP_3R2 deletion (data not shown). Taken together, our data suggest that IP_3R2, but not IP_3R1 or IP_3R3, has suppressive

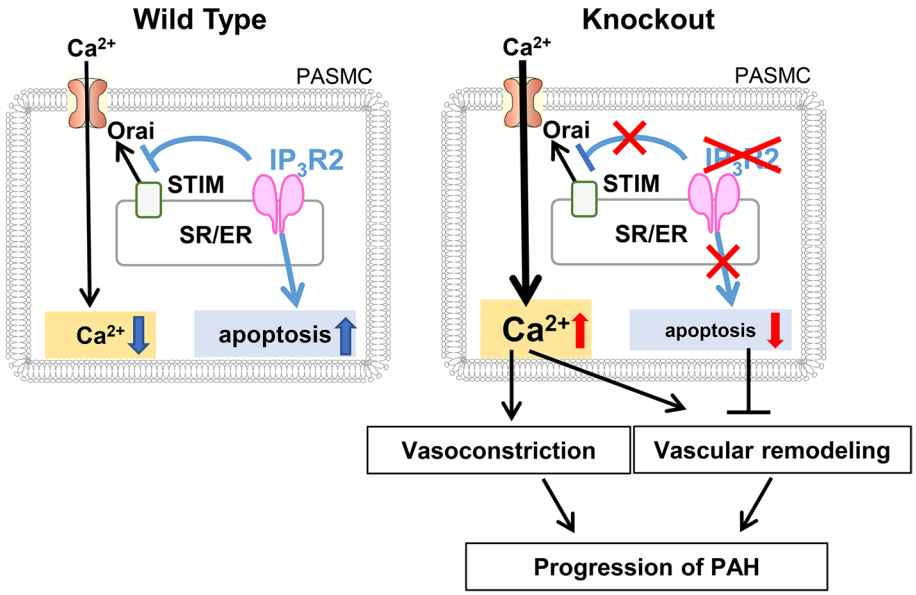

Fig. 7 Putative dual roles of IP_3R2 for apoptosis and SOCE in PASMCs to inhibit the progression of PAH. In PASMCs, IP_3R2 on SR/ER promotes apoptosis and suppresses SOCE by the inhibition of interaction between STIM and Orai, resulting in the attenuation of vasoconstriction and vascular remodeling, and eventually inhibits the progression of PAH

effect on SOCE during the progression of PAH by inhibiting STIM–Orai interactions, affecting most SOCE in PASMCs.

In this study, we showed that a loss of function of IP_3R2 in mice developed the significant aggravation of chronic hypoxia-induced PAH, possibly by the promotion of resistance to apoptosis and the enhancement of SOCE via STIM–Orai interactions in PASMCs. Our data suggest novel roles of IP_3R2, which suppresses excess Ca^{2+} influx and promotes apoptosis; these findings provide new insight into the mechanism and possible therapeutic targets for progressive PAH.

Acknowledgements The authors thank K. Fukuda who helped to develop the mouse model system of pulmonary hypertension induced by hypoxia; U. Yokoyama for the preparation of primary culture of pulmonary artery smooth muscle cells; M. Yasui for Ca^{2+} imaging with confocal microscopy. We thank Olympus Corp. for the support in Ca^{2+} imaging. The authors also thank A. Kuramochi and M. Suzuki for technical support, and members of the Division of Pediatric Cardiology in Keio University School of Medicine for helpful discussion. This work was supported by the Acterion Academia Prize 2015 to A.S. And it was also supported by Grant-in-Aid for Scientific Research from the Ministry of Education, Culture, Sports, Science and Technology, Japan to K.U. and H.Y. (Grant numbers JP19390288, JP19790740, JP21791004, JP23591583, JP26461619, JP17K10153, and JP16H05359).

Compliance with ethical standards

Conflict of interest The authors declare that they have no conflicts of interest.

References

1. Thenappan T, Ormiston ML, Ryan JJ, Archer SL (2018) Pulmonary arterial hypertension: pathogenesis and clinical management. BMJ 360:j5492
2. Kuhr FK, Smith KA, Song MY, Levitan I, Yuan JX (2012) New mechanisms of pulmonary arterial hypertension: role of Ca(2)(+) signaling. Am J Physiol Heart Circ Physiol 302:H1546–H1562
3. Archer S, Rich S (2000) Primary pulmonary hypertension: a vascular biology and translational research "Work in progress". Circulation 102:2781–2791
4. Lin MJ, Leung GP, Zhang WM, Yang XR, Yip KP, Tse CM, Sham JS (2004) Chronic hypoxia-induced upregulation of store-operated and receptor-operated Ca^{2+} channels in pulmonary arterial smooth muscle cells: a novel mechanism of hypoxic pulmonary hypertension. Circ Res 95:496–505
5. Reyes RV, Castillo-Galan S, Hernandez I, Herrera EA, Ebensperger G, Llanos AJ (2018) Revisiting the role of TRP, Orai, and ASIC channels in the pulmonary arterial response to hypoxia. Front Physiol 9:486
6. Hofmann T, Obukhov AG, Schaefer M, Harteneck C, Gudermann T, Schultz G (1999) Direct activation of human TRPC6 and TRPC3 channels by diacylglycerol. Nature 397:259–263
7. Avila-Medina J, Mayoral-Gonzalez I, Dominguez-Rodriguez A, Gallardo-Castillo I, Ribas J, Ordonez A, Rosado JA, Smani T (2018) The Complex role of store operated calcium entry pathways and related proteins in the function of cardiac, skeletal and vascular smooth muscle cells. Front Physiol 9:257
8. Putney JW (2018) Forms and functions of store-operated calcium entry mediators, STIM and Orai. Adv Biol Regul 68:88–96
9. Mikoshiba K (2015) Role of IP3 receptor signaling in cell functions and diseases. Adv Biol Regul 57:217–227
10. Berridge MJ (2016) The inositol trisphosphate/calcium signaling pathway in health and disease. Physiol Rev 96:1261–1296
11. Wojcikiewicz RJ (1995) Type I, II, and III inositol 1,4,5-trisphosphate receptors are unequally susceptible to down-regulation and are expressed in markedly different proportions in different cell types. J Biol Chem 270:11678–11683
12. Klar J, Hisatsune C, Baig SM, Tariq M, Johansson AC, Rasool M, Malik NA, Ameur A, Sugiura K, Feuk L, Mikoshiba K, Dahl N (2014) Abolished InsP3R2 function inhibits sweat secretion in both humans and mice. J Clin Invest 124:4773–4780
13. Inaba T, Hisatsune C, Sasaki Y, Ogawa Y, Ebisui E, Ogawa N, Matsui M, Takeuchi T, Mikoshiba K, Tsubota K (2014) Mice lacking inositol 1,4,5-trisphosphate receptors exhibit dry eye. PLoS One 9:e99205

14. Futatsugi A, Nakamura T, Yamada MK, Ebisui E, Nakamura K, Uchida K, Kitaguchi T, Takahashi-Iwanaga H, Noda T, Aruga J, Mikoshiba K (2005) IP3 receptor types 2 and 3 mediate exocrine secretion underlying energy metabolism. Science 309:2232–2234
15. Nakayama H, Bodi I, Maillet M, DeSantiago J, Domeier TL, Mikoshiba K, Lorenz JN, Blatter LA, Bers DM, Molkentin JD (2010) The IP3 receptor regulates cardiac hypertrophy in response to select stimuli. Circ Res 107:659–666
16. Uchida K, Aramaki M, Nakazawa M, Yamagishi C, Makino S, Fukuda K, Nakamura T, Takahashi T, Mikoshiba K, Yamagishi H (2010) Gene knock-outs of inositol 1,4,5-trisphosphate receptors types 1 and 2 result in perturbation of cardiogenesis. PLoS One 5:e12500
17. Nakazawa M, Uchida K, Aramaki M, Kodo K, Yamagishi C, Takahashi T, Mikoshiba K, Yamagishi H (2011) Inositol 1,4,5-trisphosphate receptors are essential for the development of the second heart field. J Mol Cell Cardiol 51:58–66
18. Uchida K, Nakazawa M, Yamagishi C, Mikoshiba K, Yamagishi H (2016) Type 1 and 3 inositol trisphosphate receptors are required for extra-embryonic vascular development. Dev Biol 418:89–97
19. Narayanan D, Adebiyi A, Jaggar JH (2012) Inositol trisphosphate receptors in smooth muscle cells. Am J Physiol Heart Circ Physiol 302:H2190–H2210
20. Kawakami T, Kanazawa H, Satoh T, Ieda M, Ieda Y, Kimura K, Mochizuki H, Shimada T, Yokoyama C, Ogawa S, Tanabe T, Fukuda K (2007) AAV-PGIS gene transfer improves hypoxia-induced pulmonary hypertension in mice. Biochem Biophys Res Commun 363:656–661
21. Levy PT, Patel MD, Groh G, Choudhry S, Murphy J, Holland MR, Hamvas A, Grady MR, Singh GK (2016) Pulmonary artery acceleration time provides a reliable estimate of invasive pulmonary hemodynamics in children. J Am Soc Echocardiogr 29:1056–1065
22. Gomez O, Okumura K, Honjo O, Sun M, Ishii R, Bijnens B, Friedberg MK (2018) Heart rate reduction improves biventricular function and interactions in experimental pulmonary hypertension. Am J Physiol Heart Circ Physiol 314:H542–H551
23. Yamagishi H, Olson EN, Srivastava D (2000) The basic helix-loop-helix transcription factor, dHAND, is required for vascular development. J Clin Investig 105:261–270
24. Yokoyama U, Minamisawa S, Adachi-Akahane S, Akaike T, Naguro I, Funakoshi K, Iwamoto M, Nakagome M, Uemura N, Hori H, Yokota S, Ishikawa Y (2006) Multiple transcripts of Ca^{2+} channel alpha1-subunits and a novel spliced variant of the alpha1C-subunit in rat ductus arteriosus. Am J Physiol Heart Circ Physiol 290:H1660–H1670
25. Nakamura K, Hamada K, Terauchi A, Matsui M, Nakamura T, Okada T, Mikoshiba K (2013) Distinct roles of M1 and M3 muscarinic acetylcholine receptors controlling oscillatory and non-oscillatory $[Ca^{2+}]$ i increase. Cell Calcium 54:111–119
26. Miyauchi T, Yamamoto H, Abe Y, Yoshida GJ, Rojek A, Sohara E, Uchida S, Nielsen S, Yasui M (2015) Dynamic subcellular localization of aquaporin-7 in white adipocytes. FEBS Lett 589:608–614
27. Jozsef L, Tashiro K, Kuo A, Park EJ, Skoura A, Albinsson S, Rivera-Molina F, Harrison KD, Iwakiri Y, Toomre D, Sessa WC (2014) Reticulon 4 is necessary for endoplasmic reticulum tubulation, STIM1-Orai1 coupling, and store-operated calcium entry. J Biol Chem 289:9380–9395
28. Goto J, Suzuki AZ, Ozaki S, Matsumoto N, Nakamura T, Ebisui E, Fleig A, Penner R, Mikoshiba K (2010) Two novel 2-aminoethyl diphenylborinate (2-APB) analogues differentially activate and inhibit store-operated Ca(2+) entry via STIM proteins. Cell Calcium 47:1–10
29. Hendron E, Wang X, Zhou Y, Cai X, Goto J, Mikoshiba K, Baba Y, Kurosaki T, Wang Y, Gill DL (2014) Potent functional uncoupling between STIM1 and Orai1 by dimeric 2-aminodiphenyl borinate analogs. Cell Calcium 56:482–492
30. Klinger JR, Warburton RR, Pietras LA, Smithies O, Swift R, Hill NS (1999) Genetic disruption of atrial natriuretic peptide causes pulmonary hypertension in normoxic and hypoxic mice. Am J Physiol 276:L868–L874
31. Ogawa A, Firth AL, Smith KA, Maliakal MV, Yuan JX (2012) PDGF enhances store-operated Ca2+ entry by upregulating STIM1/Orai1 via activation of Akt/mTOR in human pulmonary arterial smooth muscle cells. Am J Physiol Cell Physiol 302:C405–C411
32. Yadav VR, Song T, Mei L, Joseph L, Zheng YM, Wang YX (2018) PLCgamma1-PKCepsilon-IP3R1 signaling plays an important role in hypoxia-induced calcium response in pulmonary artery smooth muscle cells. Am J Physiol Lung Cell Mol Physiol 314:L724–L735
33. Joseph SK, Hajnoczky G (2007) IP3 receptors in cell survival and apoptosis: Ca^{2+} release and beyond. Apoptosis 12:951–968
34. Lencesova L, Krizanova O (2012) IP(3) receptors, stress and apoptosis. Gen Physiol Biophys 31:119–130
35. Akl H, Monaco G, La Rovere R, Welkenhuyzen K, Kiviluoto S, Vervliet T, Molgo J, Distelhorst CW, Missiaen L, Mikoshiba K, Parys JB, De Smedt H, Bultynck G (2013) IP3R2 levels dictate the apoptotic sensitivity of diffuse large B-cell lymphoma cells to an IP3R-derived peptide targeting the BH4 domain of Bcl-2. Cell Death Dis 4:e632
36. Zhong F, Harr MW, Bultynck G, Monaco G, Parys JB, De Smedt H, Rong YP, Molitoris JK, Lam M, Ryder C, Matsuyama S, Distelhorst CW (2011) Induction of Ca(2)+-driven apoptosis in chronic lymphocytic leukemia cells by peptide-mediated disruption of Bcl-2-IP3 receptor interaction. Blood 117:2924–2934
37. Yu Y, Fantozzi I, Remillard CV, Landsberg JW, Kunichika N, Platoshyn O, Tigno DD, Thistlethwaite PA, Rubin LJ, Yuan JX (2004) Enhanced expression of transient receptor potential channels in idiopathic pulmonary arterial hypertension. Proc Natl Acad Sci USA 101:13861–13866
38. Song MY, Makino A, Yuan JX (2011) STIM2 contributes to enhanced store-operated Ca entry in pulmonary artery smooth muscle cells from patients with idiopathic pulmonary arterial hypertension. Pulm Circ 1:84–94
39. Pan Z, Brotto M, Ma J (2014) Store-operated Ca^{2+} entry in muscle physiology and diseases. BMB Rep 47:69–79
40. Venkatachalam K, van Rossum DB, Patterson RL, Ma HT, Gill DL (2002) The cellular and molecular basis of store-operated calcium entry. Nat Cell Biol 4:E263–E272
41. Ng LC, O'Neill KG, French D, Airey JA, Singer CA, Tian H, Shen XM, Hume JR (2012) TRPC1 and Orai1 interact with STIM1 and mediate capacitative Ca(2+) entry caused by acute hypoxia in mouse pulmonary arterial smooth muscle cells. Am J Physiol Cell Physiol 303:C1156–C1172
42. Lur G, Sherwood MW, Ebisui E, Haynes L, Feske S, Sutton R, Burgoyne RD, Mikoshiba K, Petersen OH, Tepikin AV (2011) InsP(3)receptors and Orai channels in pancreatic acinar cells: co-localization and its consequences. Biochem J 436:231–239